# Aerodynamic Optimization Study of a Coaxial Rotor in Hovering Flight

Monica Syal
*Graduate Research Assistant*

J. Gordon Leishman*
*Minta Martin Professor of Engineering*

*Department of Aerospace Engineering, University of Maryland, College Park, MD*

**A primary design goal with a coaxial rotor is to minimize the combined sources of losses on the upper and lower rotors that have their source in aerodynamic interference. To this end, parametric studies were conducted using a free-vortex wake method to study the aerodynamic interference effects of changing interrotor spacing, blade twist rates, and blade planform on the interdependent loads produced on the upper and lower rotors, respectively. A formal, multistep optimization process was then conducted by coupling the aerodynamic method to an optimization approach based on the method of feasible directions, the goal being to expeditiously find the individual blade geometries that would give the highest levels of efficiency from the coaxial as a system. Because of the inherent aerodynamic differences between the upper and lower rotors of a coaxial, it is shown that the best performing coaxial rotors may require the use of different blade shapes on each rotor, but substantially different blade designs may also achieve similar values of aerodynamic efficiency. It is also shown that the nonconvexity of the design problem for a coaxial rotor may limit the usefulness of formal optimization methods, and extensive parametric studies may still be required in the process of design.**

## Principal Symbols

| | |
|---|---|
| $A$ | rotor disk area (per rotor) |
| $C_d$ | sectional drag coefficient |
| $C_{d_0}$ | minimum (zero-lift) profile drag coefficient |
| $C_P$ | rotor power coefficient, $= P/\rho A\Omega^3 R^3$ |
| $C_{P_i}$ | rotor induced power coefficient, $= P_i/\rho A\Omega^3 R^3$ |
| $C_{P_0}$ | rotor profile power coefficient, $= P_0/\rho A\Omega^3 R^3$ |
| $C_T$ | rotor thrust coefficient, $= T/\rho A\Omega^2 R^2$ |
| $C_{T_{\text{req}}}$ | target thrust coefficient of the coaxial rotor |
| $c$ | blade chord |
| $DL$ | disk loading, $= T/A$ |
| $F$ | objective function |
| $FM$ | figure of merit |
| $g_j$ | $j$th inequality constraint |
| $h$ | equality constraint |
| $N$ | number of design variables |
| $N_b$ | number of blades per rotor |
| $P$ | rotor power |
| $P_i$ | induced power |
| $P_0$ | profile power |
| $PL$ | power loading, $= T/P$ |
| $R$ | rotor radius |
| $r$ | nondimensional radial distance |
| $r_b$ | nondimensional radial breakpoint |
| $s$ | interrotor spacing |
| $T$ | rotor thrust |
| $TR$ | taper ratio of blade |
| $t$ | time |
| $\mathbf{U}$ | total induced velocity |
| $V_{\text{tip}}$ | tip speed |
| $\mathbf{X}$ | vector of design variables |
| $x, y, z$ | Cartesian coordinates |
| $\Gamma_v$ | circulation |
| $\theta$ | blade pitch |
| $\theta_{\text{tw}}$ | linear blade twist |
| $\theta_0$ | reference (collective) blade pitch |
| $\kappa_{\text{int}}$ | interference-induced power factor |
| $\rho$ | air density |
| $\sigma_e$ | thrust-weighted equivalent solidity |
| $\Omega$ | angular rotational velocity |

*Corresponding author; email: leishman@umd.edu.
Manuscript received January 2010; accepted May 2012.

## Introduction

There has been renewed interest in contrarotating coaxial rotor systems for use on helicopters, tiltrotors, and micro air vehicles; see, for example, Refs. 1–3. When used on a helicopter, a coaxial rotor has two important advantages: (1) It eliminates the need for a separate antitorque system, and (2) overall rotor diameter can be reduced relative to that of a single rotor to produce the same net thrust with the same (or similar) disk and blade loadings. Both of these advantages can lead to an aircraft of smaller size, although not necessarily one

 

that is aerodynamically more efficient or has other benefits. There may be advantages in using a coaxial rotor for a compounded advancing blade concept (Refs. 1, 4, 5), which can achieve higher forward speeds compared to a conventional helicopter. A coaxial proprotor may also have certain advantages for a tiltrotor (Ref. 2), including better aerodynamic and weight efficiencies, as well as more robust operating margins (Refs. 6, 7).

One aerodynamic issue with a coaxial rotor is that the flows from the upper and lower rotors interact, i.e., there is a reciprocal aerodynamic effect of one rotor upon the other. It is obvious that the lower rotor of the coaxial operates in at least some fraction of the slipstream from the upper rotor, usually resulting in significant adverse effects on its blade loads and performance. Larger interrotor plane spacings may help to reduce such interference losses, but this design option can lead to high parasitic drag from the exposed shaft and controls between the rotors when the system is in edgewise forward flight. Nevertheless, taking into account the reciprocal interference losses induced by one rotor on the other suggests that, at least as a hovering platform, a helicopter powered by a coaxial rotor can be of comparable aerodynamic efficiency to one using a conventional single main rotor and tail rotor. The advantages of a coaxial may become increasingly attractive if the blade shapes can be optimized to minimize the combined sources of induced, profile, and interference losses and their various interdependencies. Obviously, the trades on rotor system weight and other factors will also need to be considered in the design process.

Coleman (Ref. 8) has summarized aerodynamic research on coaxial rotors, with a review of performance characteristics, wake behavior, and suggested methods of analysis. Recent experimental work on a coaxial rotor has been conducted by McAlister et al. (Refs. 9, 10), confirming the difficulties in accurately quantifying rotor performance and in measuring the interacting rotor flow fields, but also providing more measurements for validating predictive methods. To this end, there are various theoretical and modeling approaches used to predict coaxial performance (Refs. 11–17). More recently, the momentum and blade element momentum theories for a coaxial rotor have been revisited and formalized (Refs. 15–17). Better definitions of the figure of merit for a coaxial rotor have also been developed (Ref. 15), correcting previous misinterpretations (Ref. 18). Studies of coaxial rotors using computational fluid dynamics (CFD) is a more recent endeavor (Refs. 19, 20) but are impeded by the numerical difficulties in preserving the wake vorticity before it reaches the lower rotor, as well as high computational costs. Nevertheless, CFD probably offers the best long-term approach for accurately quantifying the various sources of aerodynamic nonlinearities on coaxial rotors arising from rotor-on-rotor interference.

Previous investigations of coaxial rotor performance have not yet established firm design guidelines that can be used to help maximize (or otherwise optimize) the aerodynamic performance of a coaxial rotor to achieve the required levels of performance. Such guidelines may not parallel the procedures used for the design of single rotors. Any approach used must represent several complex and nonlinear interdependent influences, including the non-ideal induced losses that originate from the interactions between the wakes from the two rotors of the coaxial system. Other coupling effects between the two rotors, including the effects of thrust sharing and/or torque balancing between the two rotors, must also be considered. Unbalanced thrust sharing also means that each rotor will generally operate at different aerodynamic efficiencies. Consequently, any improvement in aerodynamic efficiency from any one rotor of the pair does not guarantee that improvements in overall aerodynamic efficiency will be obtained from the coaxial as a system. Furthermore, a practical coaxial rotor design may face several other constraints, including allowable rotor plane spacing to prevent blade collisions, overall rotor size, maximum feasible blade twist, tip speed, and maximum rotor weight.

The goal of the present work was to develop a methodology to aid in the understanding of how to extract the highest levels of aerodynamic performance from a coaxial rotor as a system. The methodology was also coupled into a formal optimization method, the goal being to more expediently find the required rotor geometry with the best levels of efficiency. While the current article is focused on a discussion of coaxial rotors in hovering flight conditions, the analysis is not restricted to such.

## Aerodynamic Methodologies

Attempts to optimize blade shapes on a coaxial rotor must be performed using a robust and computationally efficient methodology that includes aerodynamic models of sufficient fidelity to represent the basic flow physics. To this end, validation of the aerodynamic modeling approaches is the key. Two methods were used in the present work for the aerodynamic analysis: (1) blade element momentum theory (BEMT) and (2) the free vortex method (FVM). However, the overall structure of the optimization approach is not limited to the use of just these methods. In addition, the simple momentum theory (SMT) was used in this study to help set the performance goals that would help to extract the maximum possible aerodynamic performance from a coaxial rotor in hovering flight; coaxial interference losses cannot be reduced through blade design changes below the thresholds set by the SMT (Ref. 15).

The BEMT is a mathematically parsimonious, computationally expedient, and well-validated methodology that provides a robust theoretical basis from which to initiate a rotor design solution. However, the approach is fundamentally linear because it assumes the validity of superposition. The FVM is a higher fidelity model (albeit still inviscid) that gives a better predictive capability for the local blade loads and, therefore, it is a more rigorous basis from which to perform the blade shape optimization. Because of the much higher relative computational cost of the FVM, in an optimization process a good estimate of the initial blade design is required to ensure proper convergence and also to conserve computer resources. In some cases, this initial value can be provided by the BEMT. Further refinements to the blade design could be performed by using certain types of CFD (Refs. 19, 20), but CFD was not used in the present work.

### BEMT

The BEMT invokes an equivalence between the circulation and momentum theories of lift. First used for helicopter rotors by Gessow (Ref. 21) and Gessow and Myers (Ref. 22), it was extended to hovering coaxial rotors by Leishman and Ananthan (Ref. 16). Rand and Khromov (Ref. 17) give another implementation of the same approach. The BEMT provides a better modeling capability than the SMT because it allows the effects of blades with different planform shapes and twist distributions to be examined, at least within the limits of the assumptions of a linear theory. In fact, a major assumption in the BEMT is that the combined flow through the upper and lower rotors of a coaxial can be obtained by linear superposition of the respective flow fields, the equations governing the inflow distribution on both rotors being derived by using the same principles used in the development of the single rotor theory (Refs. 21–23). Unlike the SMT, however, which assumes uniform inflow over the rotor disk, the BEMT is a two-dimensional theory that can predict the nonuniform inflow distributions over the blades.

In the BEMT, it is assumed that successive annuli on any one-rotor disk have no mutual influence on each other, a justifiable assumption for high-aspect-ratio blades except at the blade tip (Refs. 24, 25). The outflow from the upper rotor of the coaxial will affect the inflow into the lower rotor depending upon the contraction area of its slipstream; this contraction can be determined using various assumptions and can also be generalized semiempirically to account for interrotor spacing effects (Refs. 16, 17). The lower rotor affects the upper rotor through the need to operate at both a thrust and torque trim, although other assumptions for trim may be invoked (Ref. 17). Tip effects can be included in the conventional manner into the coaxial version of the BEMT using a Prandtl tip loss factor, with the inflow angle in this case being calculated based on the combined rotor flows.

**Free-vortex method**

The many factors influencing the nature of the flow in the interference region between the upper and lower rotors means that a FVM should provide a better fidelity in defining the aerodynamic environment. A FVM representation of the coaxial is shown in Fig. 1. The crux of any vortex theory is in convecting the resulting wake vorticity as accurately as possible. In the present implementation of the FVM, the vorticity behind each blade was assumed to be composed of two parts: a near wake and a far wake. The rotor was modeled as two sets of rigid, articulated blades. The blades were represented using a Weissinger-L type model with a full span near wake (truncated at 30° behind each blade) to provide the compatibility condition with the free wake (Ref. 26). Single vortex filaments, extending up to six rotor revolutions in length, were used to represent the free vortex wake behind each blade in this case, but the FVM is not limited to using tip vortices alone; justification of what is actually needed is obtained through validation with experiments and/or other models. Modeling the tip vortices also significantly reduces the computational costs by limiting the total number of velocity field computations that need to be performed numerically when using the Biot–Savart law, which becomes particularly important when the FVM is used in an optimization context. The strength and radial release point of tip vortices depend upon the blade lift distribution and vary with blade azimuth location. In the present formulation, the tip vortex strength was equal to the maximum bound circulation over the span of the blade with a release point at the blade tip.

Fundamentally, the convection of the vortical wake is governed by the three-dimensional, incompressible Navier–Stokes equations, which under the assumptions of irrotational and incompressible flow can be written in the form of a vorticity transport equation. In blade-fixed coordinates, the governing equation for the wake becomes an advection equation, which determines the movement of the wake filaments under the given conditions. In the present FVM approach, the governing equation for the wake displacements is then discretized in space and time and solved using a five-point central difference discretization in space and a two-point backward difference discretization in time (Refs. 26, 27); discretizations of 10° in space and time were used in the present work. These numerical discretizations are second-order accurate and are consistent with the accuracy obtained with the velocity field reconstruction made using the Biot–Savart law (Ref. 28). The semiempirical vortex Reynolds number dependent model incorporated into the FVM accounts for changes in vorticity resulting from diffusion (Ref. 29) as well as from filament stretching (Ref. 30). After calculating the positions of the wake markers in space and as a function of time, the inflow velocities and the resulting distributions of airloads on each blade follow, using the conventional blade element approach. The aerodynamics at the blade sections were modeled by using generalizations derived from measured properties of the NACA 0012 airfoil (Ref. 31).

**Coaxial rotor trim methodology**

Because a coaxial rotor generally operates at a torque-balanced condition at a specified system thrust or weight, each rotor must be trimmed by adjusting its individual reference blade pitch values. The individual blade flapping moments, rotor thrust, and torque were obtained by integrating the airloads over the blade span and around the rotor azimuth. Because the blade flapping response determines the wake/blade attachment boundary condition, it necessitates the tight coupling of the blade flapping motion to the rotor wake solution. The collective pitch on the rotors is then adjusted iteratively until the required thrust is generated,

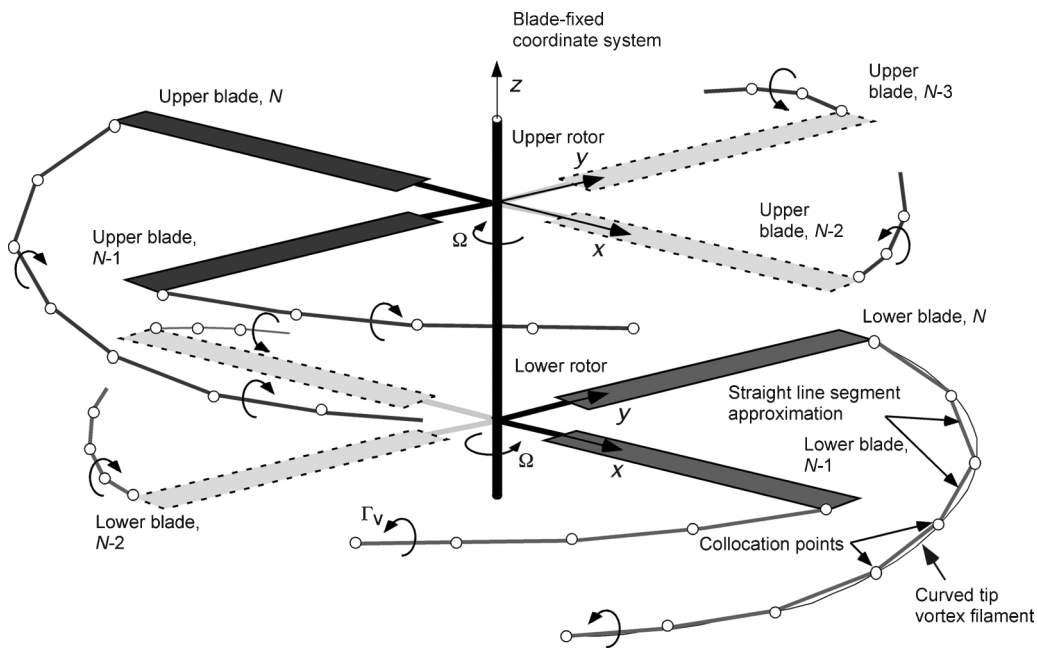


**Fig. 1. Flow model used for the FVM applied to a coaxial rotor.**

i.e., $\Delta C_T = \{C_{T_{\text{req}}} - (C_{T_u} + C_{T_l})\} \rightarrow 0$, and the torque-balanced operating condition is reached, i.e., $\Delta C_P = (C_{P_u} - C_{P_l}) \rightarrow 0$, within the specified tolerance. During this coupling process, the upper and lower rotors are continuously trimmed using collective and cyclic blade pitch inputs to obtain a converged performance solution at the specified flight condition with the needed thrust and also at a torque balance. Typically, a tolerance of $10^{-4}$ is used on the root mean square of changes in $C_T$ and $C_P$. Further details on the trimming process for a coaxial rotor are given in Refs.32 and 33.

## Optimization Methodology

The general goal is to find a blade design such that the induced and profile losses are minimized with the objective of maximizing the overall aerodynamic efficiency of the rotor. However, the final rotor design must be achieved by balancing the overall performance goals needed for each and every vehicle to which the rotor is attached. As previously explained, the performance optimization of a coaxial rotor poses a more challenging problem, mainly because of the effects of rotor-on-rotor aerodynamic interference and the sensitivity of such interference to thrust and forward speed. While it is obvious that the wake from upper rotor will affect the aerodynamics of the lower rotor, it is less clear how the lower rotor affects the performance of the upper rotor, except when the two rotors are very closely spaced, in which case interference effects will be strong. However, even if there are limited wake interactions, the two rotors of a coaxial system are always aerodynamically coupled to some degree because they will usually operate at a torque balance for trimmed flight conditions; the different flow environments on the upper and lower rotors mean they will generally share a different proportion of the total thrust.

The blade shape optimization process can be formalized in terms of a set of $N$ suitably chosen rotor design variables $\mathbf{X} = x_1, x_2, \ldots, x_N$ that can be used to minimize (or maximize) a specified aerodynamic performance related objective function, subject to certain constraints, e.g., find $\mathbf{X}$ such that

$$F(\mathbf{X}) \rightarrow \min \tag{1}$$

subject to

$$g_j(\mathbf{X}) \leq 0 \qquad j = 1, 2, \ldots, M \tag{2}$$

$$h_k(\mathbf{X}) = 0 \qquad k = 1, 2, \ldots, L \tag{3}$$

and when imposing the bounds

$$\mathbf{X}_i^l \leq \mathbf{X}_i \leq \mathbf{X}_i^u \qquad i = 1, 2, \ldots, N. \tag{4}$$

Equations (2)–(4) define the set of constraints that should be satisfied. The portion of the design space in which all the inequality $g_j(\mathbf{X})$ and equality $h_k(\mathbf{X})$ constraints are satisfied then defines the feasible solution region. Equation (4) defines the side constraints, i.e., the allowable upper and lower limits of the chosen rotor design variables. Notice that if the optimization problem requires $F(\mathbf{X})$ to be maximized instead of minimized, then the formulation remains valid by simply replacing $F(\mathbf{X})$ with $-F(\mathbf{X})$.

Established design practices show that the rotor diameter, tip speed, blade twist, taper (planform), and airfoil section are the primary design variables that must be selected to attain a specified level of rotor performance. In the case of a coaxial rotor, the possibility of using different blade shapes for both the upper and the lower rotors must be considered; there can be no expectation that the resulting blade sets will be exactly of the same shape if extracting the maximum aerodynamic efficiency from the coaxial as a system is the ultimate goal. Because of the need to minimize rotor-on-rotor interference, interrotor spacing becomes another design variable for a coaxial. However, the range of practical spacings for a coaxial rotor (at least when used on a helicopter) may be dictated by other constraints that may limit aerodynamic performance. For example, side constraints limiting the attainable performance may include the vertical dimensions of the rotor system or of the vehicle, or the maximum rotor diameter (e.g., for storage or transportation), or the need to have sufficiently high interrotor spacings to avoid collisions between the contrarotating blades at extreme flapping angles.

### Method of feasible directions

The design of the blade shapes becomes a constrained optimization problem; the actual constraints used in the present work for the coaxial rotor will be defined later. Optimization of a constrained problem can be performed using established methods such as the method of feasible directions (MFD), sequential quadratic programming (SQP), or probabilistic algorithms (Ref. 34). In the present work, the MFD was selected for the optimization (Ref. 35), primarily because it provides faster convergence in comparison with probabilistic algorithms. The MFD is based on finding a feasible/usable search direction $\mathbf{S}^k$ (where $k$ is an intermediate step in the optimization), which reduces the value of an appropriately chosen objective function $F(\mathbf{X}^k)$, while also keeping the design vector inside the feasible region. Mathematically, a feasible direction should satisfy the condition

$$\nabla g_j(\mathbf{X}^k) \cdot \mathbf{S}^k \leq 0 \tag{5}$$

for all the constraints that are active at $\mathbf{S}^k$.

The MFD algorithm consists of the iterative application of two steps: (1) the determination of a feasible/usable direction and (2) a constrained one-dimensional minimization along that direction. The first step is in itself is an optimization problem that seeks to find the direction along which the objective function can be reduced while also satisfying all of the constraints. This problem is solved by using a simplex-like algorithm. The MFD applies the two steps until the changes in the design variables or the changes in the objective function fall below a specified threshold, or until the Kuhn–Tucker conditions are satisfied.

### Implementation of the MFD algorithm

The optimization of coaxial rotor can be expected to have at least some convexity, which is a situation that occurs when multiple optima are present within the defined bounds of the design variables. Like most gradient-based methods, the MFD will always converge to a local optimum for nonconvex problems; there is no guarantee, however, that the MFD will ever reach the global optimum for these problems. Therefore, the optimization process must often be repeated several times (with different initial conditions) to cover most of the anticipated design space, the final optimum being obtained by comparing the values of the local optima.

The initial blade designs for the coaxial rotor were determined using aerodynamic predictions from the BEMT. Despite the more approximate nature of these solutions (Refs. 16, 17), which may also invoke certain empirical assumptions, the excellent computational efficiency of the BEMT allows for the rapid estimation of rotor performance as a function of the primary design variables. This first "optimum" lends itself to the determination of an initial condition for the calculations using the FVM that also provides assessments of the rotor trim state. This initial condition was then used with the FVM to determine a first flow field solution, which was used as a new starting point for the blade shape optimization. The MFD method provides an updated set of design solutions, and the

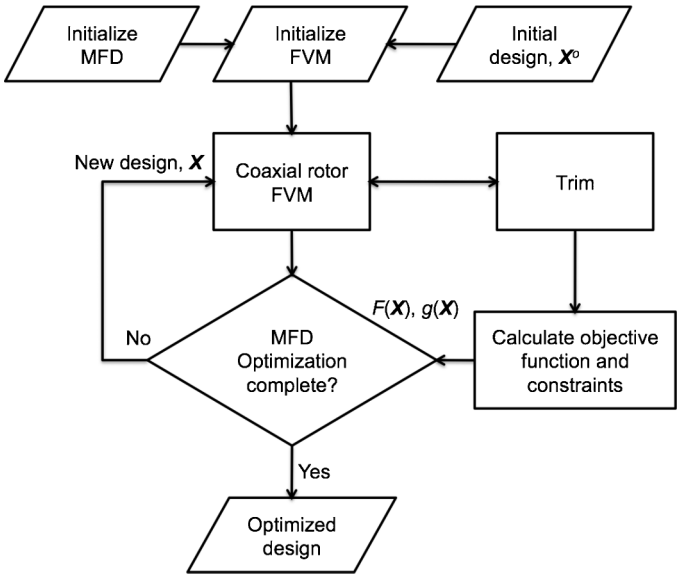


**Fig. 2. Schematic of the coupling process between the aerodynamic solution and optimization method.**

flow field and resulting rotor performance is then recomputed by using the FVM.

A flowchart of the overall optimization process is shown in Fig. 2. Notice that the trim Jacobian is recomputed for each updated rotor design, and the rotor is retrimmed accordingly. The overall process continues until aerodynamic convergence is achieved. Appropriate aerodynamic performance related objective functions can then be evaluated.

### Objective functions

The most appropriate performance metric for a rotor design in which its diameter and/or its tip speed may also be design variables is to maximize thrust generated per unit power required, i.e., to maximize the power loading $PL$. In terms of the constituent induced and profile parts of the power, the value of $PL$ for a coaxial rotor can be written as

$$PL = \frac{C_{T_{\text{req}}}}{\left[\left(C^u_{P_i} + C^l_{P_i}\right) + \left(C^u_{P_0} + C^l_{P_0}\right)\right]\Omega R} \tag{6}$$

where the superscripts in this case $u$ and $l$ refer to the upper and lower rotors, respectively.

Another possible objective function for hovering flight conditions is the figure of merit ($FM$). The $FM$ is a metric used to compare hovering performance relative to the ideal performance as given by the SMT. Because the two rotors of a coaxial share, in general, unequal thrust values when the system is operated at a torque balance, the rotors will have unequal disk loadings and aerodynamic efficiencies ($FM$ is a function of disk loading). The $FM$ for a coaxial rotor can be defined in coefficient form as

$$FM = \frac{\kappa_{\text{int}} \dfrac{C_{T_l}^{3/2}}{\sqrt{2}} \left[\left(\dfrac{C_{T_u}}{C_{T_l}}\right)^{3/2} + 1\right]}{C_{P_{\text{actual}}}} \tag{7}$$

where the ratio $C_{T_u}/C_{T_l}$ represents the thrust sharing between the upper and lower rotors and $C_{P_{\text{actual}}}$ is the actual power coefficient for the coaxial (in this case, it was calculated using the FVM). Notice that $\kappa_{\text{int}}$ represents the unavoidable induced interference losses between the two rotors, even in the ideal case, the actual quantitative value depending on basis used for comparison (Ref. 15). In the present work, $\kappa_{\text{int}} = 1.2657$, which corresponds to an ideal coaxial rotor with the lower rotor of the pair encountering the fully developed wake of the upper rotor when the system is operated at a torque balance, i.e., the minimum possible aerodynamic loss condition for a coaxial. Because the two rotors of a coaxial system operate at different aerodynamic efficiencies, which is reflected in the expression of $FM$ given by Eq. (7), this expression was used as the objective function in the present study.

The flow field around a coaxial rotor system can be aperiodic because of wake–wake and wake–blade interactions, a result also known experimentally (Ref. 10). Therefore, fluctuations can be obtained in the constituents of the objective functions (i.e., in the thrust and power) from rotor revolution to revolution even at trim. Therefore, it was sometimes difficult to establish tight numerical tolerances on the overall rotor wake convergence characteristics. In the present work, the FVM solution was considered converged when the objective function changed by less than 0.001% over five successive previous rotor revolutions. The resulting rotor performance was then used to recalculate the search direction, the optimization process being continued until $FM$ of the coaxial system was maximized.

## Results and Discussion

First, to establish predictive credibility, results from the BEMT and the FVM were compared to measurements of coaxial rotor performance as well as outcomes from other methods, where available. Second, a series of parametric studies were conducted to examine the effects of blade twist and planform shape on aerodynamic efficiency in hovering flight. Finally, a blade shape optimization exercise was conducted by using the MFD to maximize the overall efficiency of a specific coaxial rotor system in hovering flight.

### Validation and comparisons with other methods

Outcomes were first compared against rotor performance measurements made by Harrington (Ref. 36). These measurements were made for two nominally full-scale rotor systems, which are referred to as Rotor 1 and Rotor 2, respectively. Both rotor systems were 25 ft (7.62 m) in diameter with untwisted blades. Rotor 1 had two tapered blades per rotor (approximately a 3:1 taper ratio), with a thrust-weighted solidity, $\sigma$, of 0.027 (i.e., $2\sigma = 0.054$ when operated as a coaxial). Rotor 2 had two blades per rotor that were tapered only in a thickness-to-chord ratio with a solidity of 0.076 (i.e., $2\sigma = 0.152$ as a coaxial). Rotor 1 had an interrotor plane spacing of $0.186R$, and Rotor 2 had an interrotor spacing of $0.16R$.

Figure 3 shows the power polars for Rotor 1 predicted using the FVM and BEMT, which both show good agreement with the measurements. Figure 4 shows an example of the wake geometry and contours of the induced velocity field, in this case identifying the tip vortices trailed from the blades of each rotor. The wake from the upper rotor passes smoothly through the disk of the lower rotor without much loss of its helical structure; these results being consistent with the flow visualization of Taylor (Ref. 37) and McAlister et al. (Refs. 9, 10). The flow model that was assumed in the development of the BEMT (Ref. 16) is also confirmed from this wake solution.

Figure 5 shows the corresponding power polars for the Harrington Rotor 2. The results in this case were compared with predictions using a Reynolds-averaged Navier-Stokes model by Lakshminarayan and Baeder (Ref. 20). The power polars predicted using the FVM were found to be in good agreement with both the measurements and the CFD results.

Because of the unavailability of spanwise distributions of airloads on the blades, the airloads predicted by the FVM for the Harrington

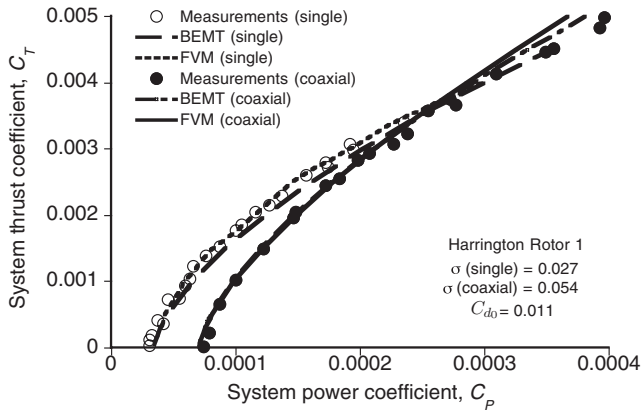


**Fig. 3. Comparison of the predicted power polars obtained using the FVM and BEMT against measurements for the Harrington Rotor 1.**

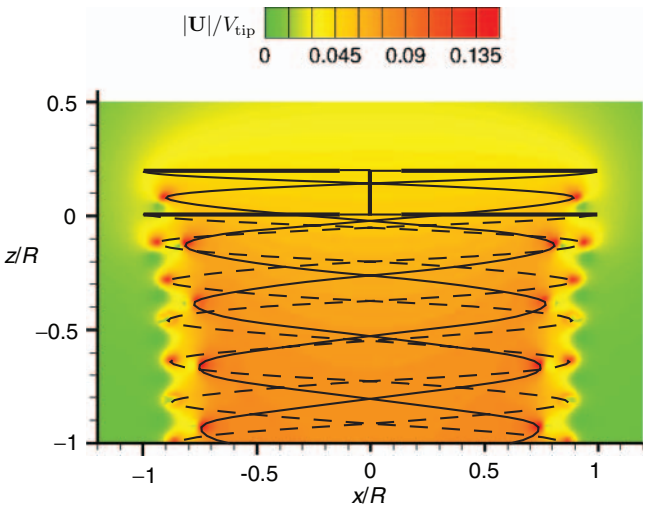


**Fig. 4. Example of the predicted flow field and vortex wake geometry (solid lines) of the Harrington Rotor 1 when operated in hover at $C_T = 0.004$; background contours show total induced velocity.**

Rotor 1 were compared with those from the BEMT, even though this latter approach is inherently linear. The BEMT calculations were performed by assuming a wake contraction ratio from the upper rotor of 0.76, which was the value predicted by the FVM in this case. Figure 6 shows the predicted thrust distribution over the upper and lower rotors using the BEMT and FVM, where at least some of the differences shown are to be expected. Notice that at the torque-balanced condition, the upper rotor carries a higher overall thrust than the lower rotor. Because of the higher inflow values over the inboard parts of the lower rotor, the blades operate at lower angles of attack there and also incur higher induced losses. (The thrust is slightly negative well inboard on the blades because of the relatively high inflow angles there and the corresponding negative angles of attack.) Over the outer part of the lower rotor, the thrust recovers to reach values nearly equal to those on the upper rotor over the same region.

Figure 7 shows the corresponding induced torque distribution over the upper and lower rotors. It is apparent that torque on the rotor is slightly greater in the regions where the wake from the upper rotor impinges upon it, which is the source of much of the induced losses on a coaxial. Recall that these calculations were performed at a torque-balanced operating state, so the areas under the torque curves of the upper and lower rotors are almost equal. Notice that the breakout for profile power

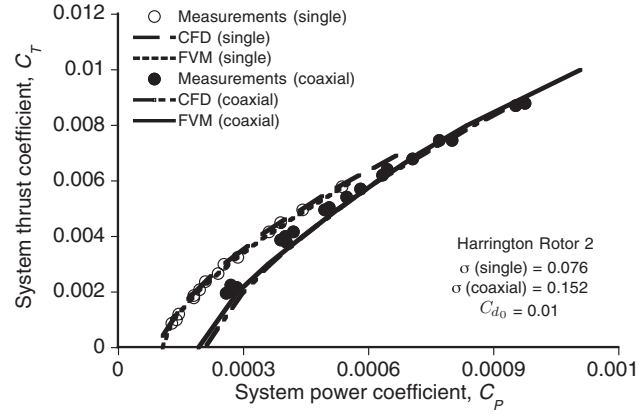


**Fig. 5. Comparison of the predicted power polars when using the FVM against both CFD results and measurements of the Harrington Rotor 2.**

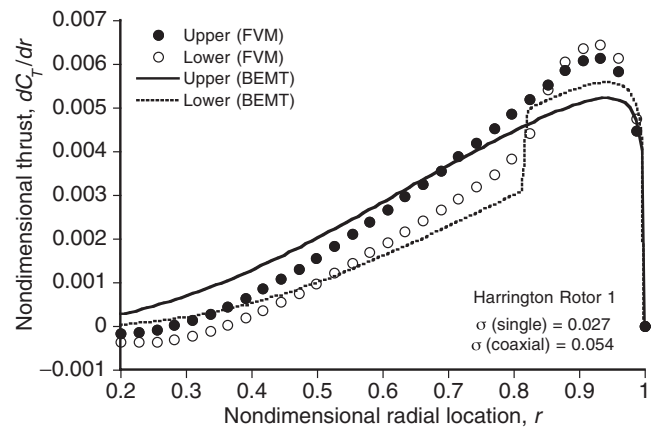


**Fig. 6. Predicted spanwise thrust distribution on the upper and lower rotors of the Harrington Rotor 1.**

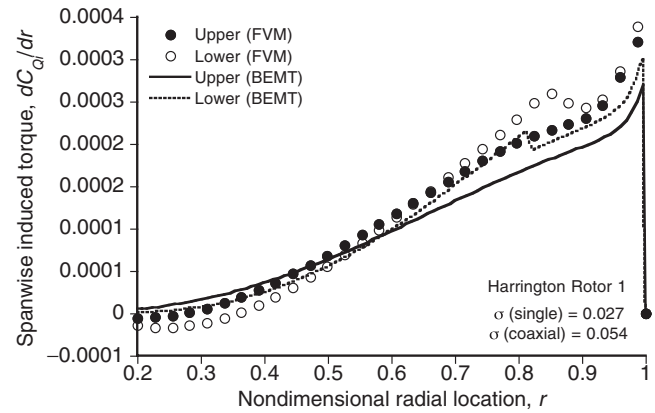


**Fig. 7. Predicted spanwise induced torque distribution on the upper and lower rotors of the Harrington Rotor 1.**

is not shown but this component comprises a much smaller portion of the total power.

Further validation was conducted with the coaxial rotor measurements of McAlister and Tung (Ref. 10). The rotor in this case had a radius of 24.35 inches and used blades of 1.95-inch chord and $-36^\circ$ twist, with a weighted solidity per rotor of 0.07647. The rotors were separated by

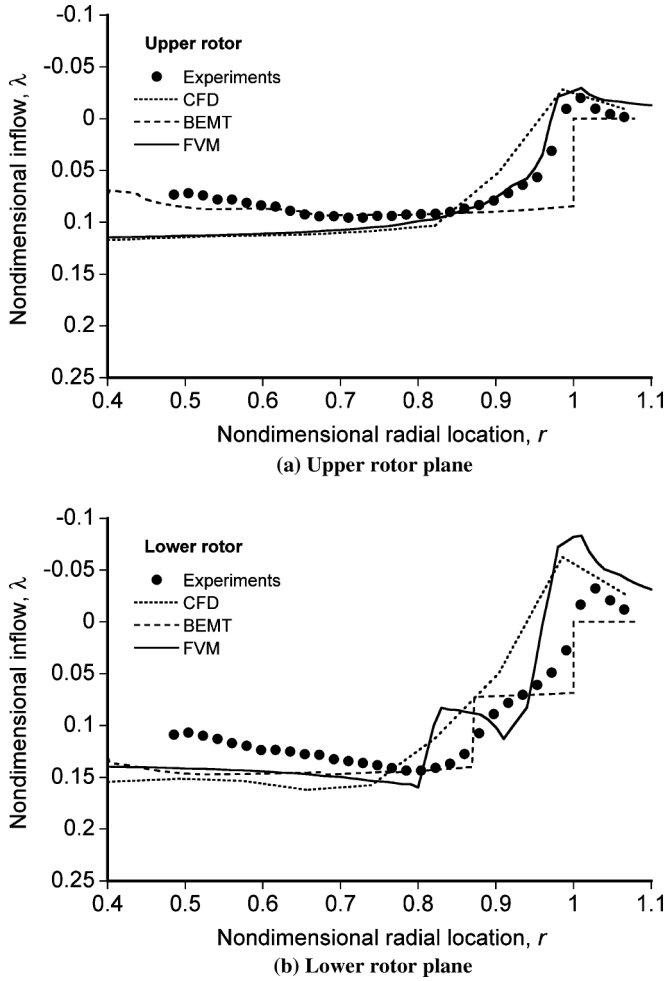


**Fig. 8. Spanwise distributions of time-averaged inflow for the McAlister and Tung coaxial rotor (Ref. 10).**

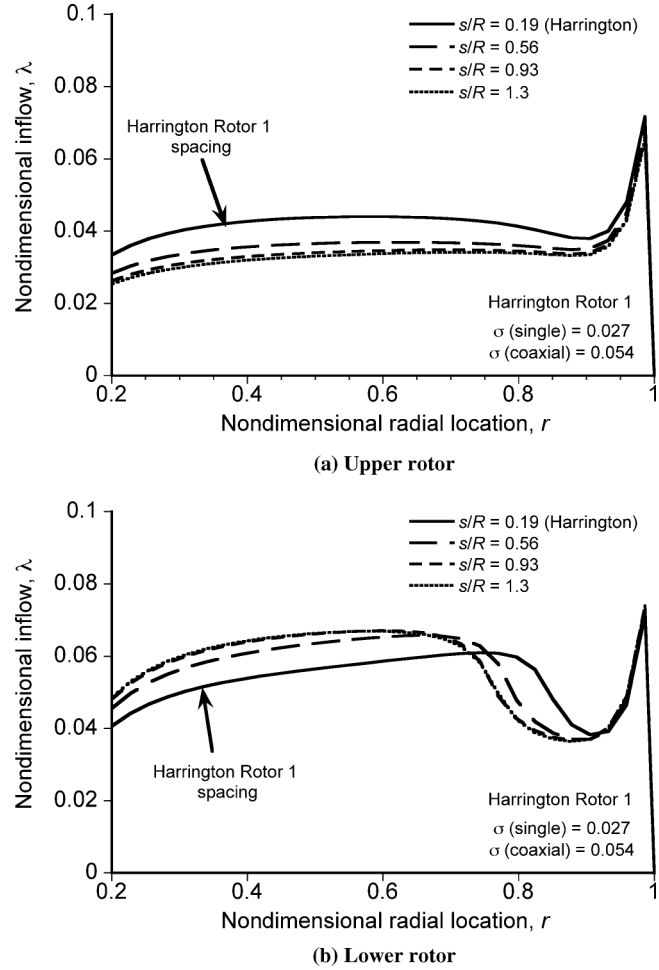


**Fig. 9. Spanwise inflow distribution on the upper and lower rotors as a function of interrotor spacing (Harrington Rotor 1).**

$0.2R$. Measurements were made at a torque-balanced condition with a system $C_T$ of 0.018. Figures 8(a) and 8(b) show the inflow distributions at the planes of upper and the lower rotors, respectively, as obtained by using the FVM, CFD (OVERFLOW2 as described by Buning (Ref. 38)) and another version of the BEMT (Ref. 17). The FVM and CFD predictions describe well the inflow at the tip region, including the upwash at the tip and the adjacent region outside, but somewhat overpredict the inflow inboard over the upper rotor. Notice that the FVM predicts steeper induced velocities when the vortex trailed by the upper rotor interacts with the blade of the lower rotor. Juhasz et al. (Ref. 39) have discussed such results in more detail.

### Blade design parametric studies

The expected nonconvexity of the design space for a coaxial rotor meant that parametric studies were needed to understand the consequences of changes to the primary design variables. These variables included interrotor spacing, blade twist on the upper and lower rotors, the respective solidities, and blade planform shapes. However, the present approach is not limited to using just these variables. Changes in overall aerodynamic efficiency from changes in any one parameter were examined while keeping all other parameters fixed. The baseline rotor geometry chosen was the Harrington Rotor 1, the analysis being performed in hovering flight at a system thrust coefficient of $C_T = 0.004$.

*Rotor-on-rotor interference assessment.* The upper and lower rotors of a coaxial affect each other in two ways. First, there is an interdependent aerodynamic coupling effect through the induced flow fields of both rotors. Second, there is a coupling because of the need to maintain an overall trim state at the torque-balanced operating condition. Figures 9(a) and 9(b) show the spanwise variations of the inflow over the upper and lower rotors, respectively, for different interrotor spacings, $s/R$, at a trimmed torque-balanced condition. As $s/R$ increases, the inflow at the upper rotor decreases; see Fig. 9(a). Simultaneously, the inflow on the lower rotor increases inboard under the influence of the wake from the upper rotor; see Fig. 9(b). This outcome is a consequence of the higher slipstream velocities in the fraction of the wake from the upper rotor encountered by the lower rotor. Over the outboard regions on the lower rotor, the inflow decreases with increasing $s/R$ because of the upwash effects from the tip vortices trailed by the upper rotor; see Fig. 9(b).

A coaxial rotor generally operates at a trimmed torque-balanced condition, so the increased torque on the lower rotor from the higher induced losses requires that more thrust be carried on the upper rotor; see Fig. 10(a). On the lower rotor, the local thrust decreases in the regions where the inflow is higher and increases outside these regions; see Fig. 10(b). These effects give a notable increase in the thrust on the upper rotor and a reduction in thrust on the lower rotor at the torque-balanced condition. (Recall that in all cases the rotor is trimmed so that the total system thrust remains constant.) At higher values of $s/R$, the thrust sharing becomes more constant but still unequal.

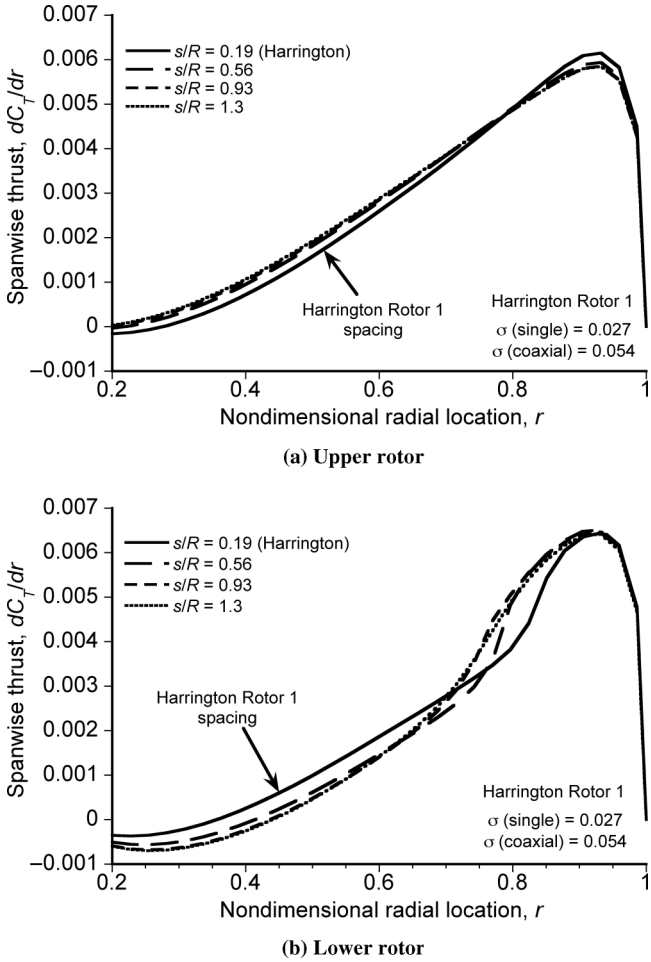


**Fig. 10. Spanwise thrust distribution on the upper and lower rotors as a function of interrotor spacing (Harrington Rotor 1).**

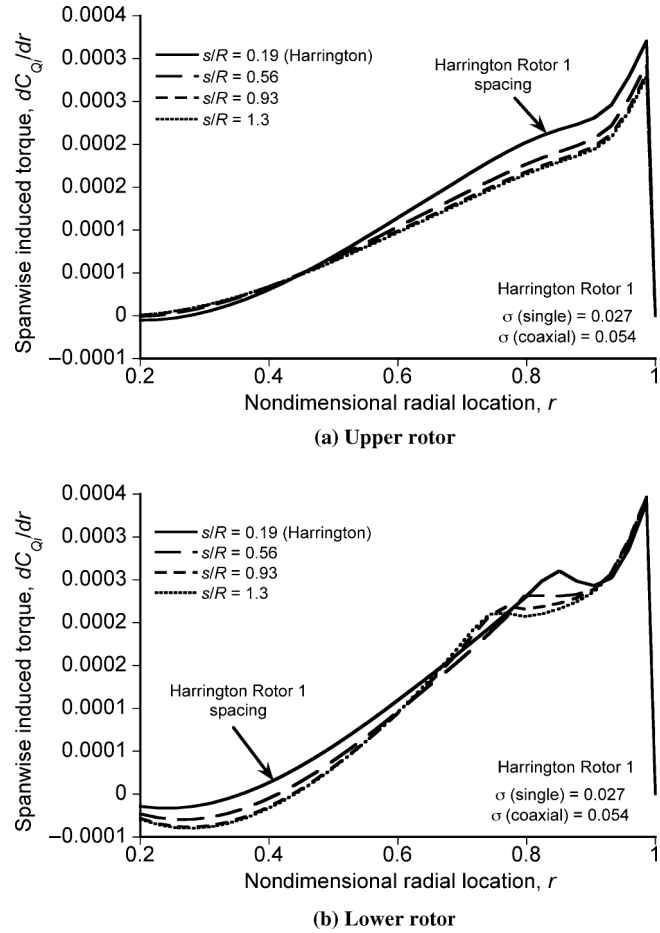


**Fig. 11. Spanwise induced torque distribution on the upper and lower rotors as a function of interrotor spacing (Harrington Rotor 1).**

Figures 11(a) and 11(b) show the variations of the spanwise distributions of the induced power for different interrotor spacings. On the inner regions of the upper rotor, the thrust loading increases and the inflow decreases with an increase in $s/R$, this effect causing almost no change in the corresponding induced power. On the outer regions of the rotor, both the thrust and the inflow were reduced, resulting in a decrease in torque over these regions. As previously explained, on the lower rotor the inflow increases and the thrust decreases over the regions of the disk that are affected by the slipstream from the upper rotor, resulting in a relative net decrease in its torque requirements. The inflow decreases and the thrust increases over the outer regions on the lower rotor, resulting again in a relative reduction in the net system torque needed at the higher values of $s/R$.

The torque required by both rotors is equal and opposite at the torque-balanced condition (assuming that the rotational speeds of both rotors are equal). Figure 12 shows that indeed the induced power reduces with an increase in $s/R$, but that the profile power remains almost constant. The values in this case are shown relative to the power obtained for the Harrington Rotor 1 at the baseline value of $s/R$. These results show that a net decrease in the total power required is obtained when the rotor is operated at higher $s/R$, the induced interference losses between the rotors being responsible for the primary effects on the performance.

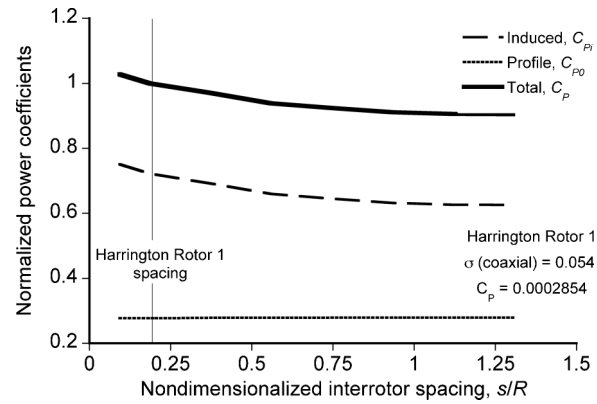


**Fig. 12. Variation of induced, profile, and total power as a function of interrotor spacing (Harrington Rotor 1).**

*Effects of the lower rotor on the upper rotor.* Each rotor of the coaxial affects the performance of the other rotor through the induced flow field and also through the overall trim requirement of the system (e.g., to maintain torque balance). It has been shown how the upper rotor affects the lower rotor but how the lower rotor affects the upper rotor is less clear. Rand and Khromov (Ref. 17) have used an ad hoc method to represent such effects, but the physical behavior is complicated. Even in the absence of any aerodynamic representation of the effects of the lower rotor on the upper rotor, the performance of the upper rotor will

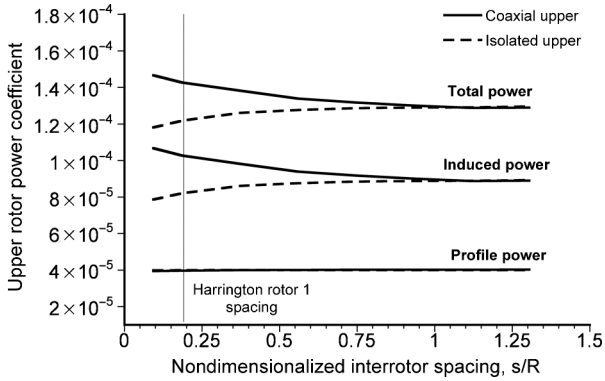


**Fig. 13. Variation of total, induced, and profile power coefficients of the upper rotor as part of the coaxial and as an isolated rotor, as a function of the interrotor spacing (Harrington Rotor 1).**

be affected by the trim state, e.g., to produce a torque balance for a given system thrust.

To study these interference effects, the upper rotor was separated and isolated from the coaxial system and then analyzed as a single rotor operated at the same thrust (and disk loading) as for the coaxial system at the torque-balanced state. By comparing the performance of the upper rotor at different interrotor spacings with the performance of this isolated rotor, the effects of the lower rotor on the aerodynamic performance of the upper rotor can be better evaluated. The isolated upper rotor was trimmed to the same thrust for such a comparison, this condition being called the equivalent single rotor.

Figure 13 shows the induced, profile, and total power coefficients for the upper rotor of the coaxial and for the equivalent single rotor for different values of $s/R$. The power of the upper rotor decreased with $s/R$ (also shown in Fig. 12). The thrust at which the equivalent single rotor was trimmed increased with $s/R$ because of the increase in the fraction of the thrust shared by the upper rotor. This outcome resulted in an increase in the power of the equivalent single rotor, as shown in Fig. 13. The difference between the power for the upper rotor of the coaxial and of the equivalent single rotor was significant for smaller values of $s/R$; see Fig. 13. These differences become negligible for higher values of $s/R$. This result confirmed that the effects of the lower rotor on the performance of the upper rotor of a coaxial cannot be neglected for smaller values of $s/R$. In this regard, the BEMT is less useful for making predictions of such effects, even when making ad hoc assumptions (Ref. 17).

*Blade twist effects.* Another study was performed to examine the interdependent effects of blade twist on the upper and lower rotors. It was shown previously that at smaller interrotor spacings, the lower rotor significantly affects the performance of the upper rotor. Therefore, changing the blade twist values on any one of the rotors will, in general, affect the performance of the entire coaxial rotor as a system. However, the resulting interdependencies from any changes in blade twist are certainly not obvious.

Reference 16 has shown that the selection of an optimum blade twist can minimize the induced losses on a coaxial rotor in the hover state. In the ideal case, hyperbolic and double hyperbolic twist distributions are needed on the blades of the upper and lower rotors, respectively. A linear twist distribution, however, is a good approximation to a hyperbolic twist distribution near the blade tips, so the effects of using different linear twist values were analyzed first. To this end, the blade twist on the upper rotor was changed from $0^\circ$ to $-30^\circ$ while holding constant the blade twist on the lower rotor.

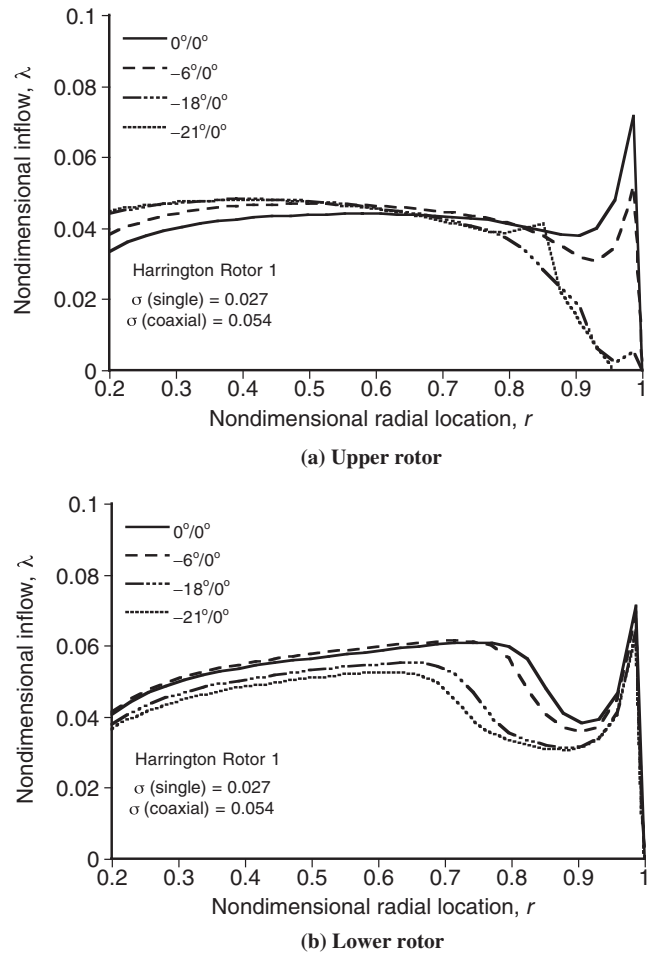


**Fig. 14. Variation of the spanwise inflow distribution on the upper and lower rotors as a function of the blade twist rate on the upper rotor (Harrington Rotor 1).**

Higher collective pitch was needed on the upper rotor when using the larger values of blade twist. Higher collective gives an increase in the inflow distribution inboard on the blades and a decrease in the inflow further outboard on the upper rotor; see Figs. 14(a) and 14(b), respectively. Notice that the legend $\theta^u_{\text{tw}}/\theta^l_{\text{tw}}$ used here denotes the linear twist rate per rotor radius for the upper and lower rotors, respectively. These results also show that for larger blade twists on the upper rotor the decrease in inflow toward the tip region is more significant than the increase in inflow further inboard. This effect resulted in a notable reduction in the inflow over most of the lower rotor, although the decrease was clearly more pronounced in the region where the wake from the upper rotor impinged upon it. Notice that for blade twists larger than $-21^\circ$ the blade tip was significantly off-loaded, which meant that the tip vortices in the wake convected more slowly away from the rotor. Consequently, the vortex filaments interacted with the passing blades and the signature of this interaction can be seen in the inflow distribution in Fig. 14(a); this effect increased slightly the induced losses thereby reducing the overall aerodynamic efficiency of the coaxial as a system.

Increasing the blade twist on the upper rotor also biased the thrust distribution to the inboard regions on the upper rotor; see Fig. 15(a). On the lower rotor, the thrust distribution remained almost constant over the inboard regions, but a slight increase in the thrust grading was obtained where the wake from the upper rotor impinged on the lower rotor; see Fig. 15(b).

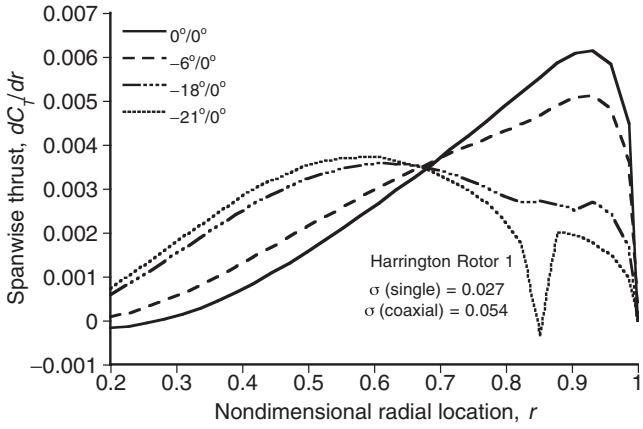


**(a) Upper rotor**

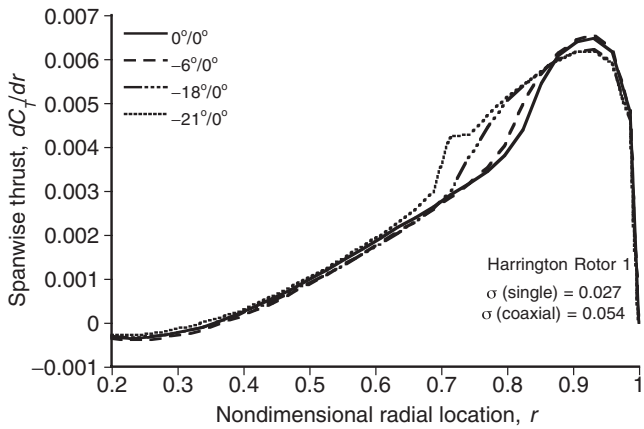


**(b) Lower rotor**

**Fig. 15. Variation of the spanwise thrust distribution on the upper and lower rotors as a function of the blade twist rate on the upper rotor (Harrington Rotor 1).**

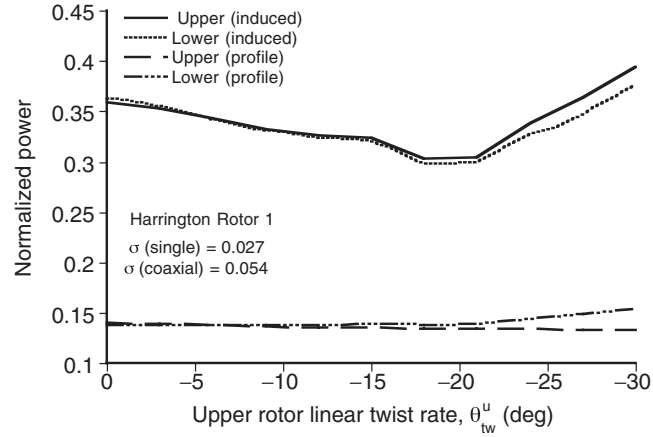


**Fig. 16. Variation of the induced and profile power contributions on the upper and lower rotors as a function of the blade twist rate on the upper rotor (Harrington Rotor 1).**

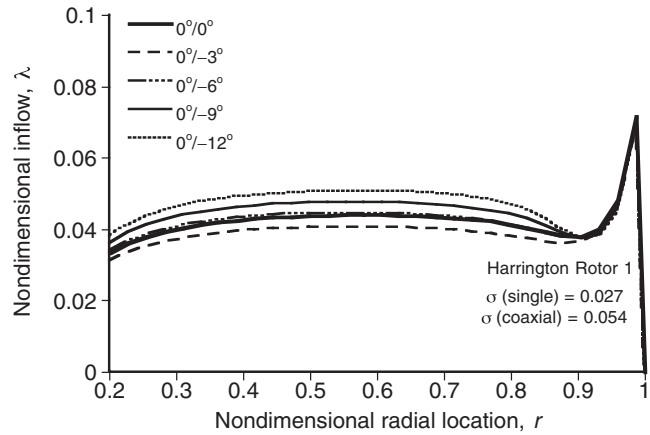


**(a) Upper rotor**

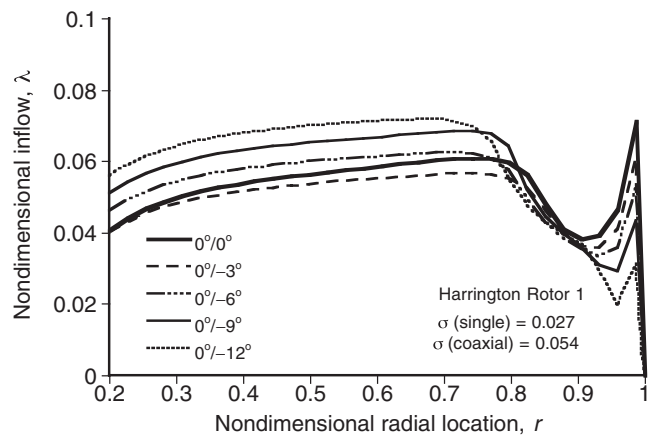


**(b) Lower rotor**

**Fig. 17. Variation of the spanwise inflow distribution on the upper and lower rotors as a function of the blade twist rate on the lower rotor (Harrington Rotor 1).**

The combined induced and profile losses on the upper and lower rotors are shown in Fig. 16. Again, the values are normalized by the total power of the baseline (Harrington Rotor 1) system. The results showed that an increase in the blade twist on the upper rotor decreases the induced losses on both rotors until a twist of $-21^\circ$ was reached. At this point, the induced losses increased quickly because of the increasing extent of nonuniform inflow and the development of nonideal thrust gradings on the blades (i.e., deviating from the more ideal triangular distributions).

Because the upper rotor in this case operates at somewhat lower angles of attack compared to the lower rotor (which has untwisted blades), the profile losses are also slightly reduced on the upper rotor and are slightly increased on the lower rotor from the effects on increasing blade twist on the upper rotor. For the higher twists used on the upper rotor (i.e., for $\theta_{tw}^{u} \leq -21^\circ$), the average inflow increases over both rotors and the collective pitch angle required to maintain a torque balance then increases on the lower rotor. This outcome increases the average angle of attack on the lower rotor and leads to an increase in the profile power with increasing blade twist; see Fig. 16. For the present configuration, the total system power reached a minimum when using a blade twist of $-18^\circ$ on the upper rotor.

A corresponding investigation was made to examine the effects of changing blade twist on the lower rotor, in this case by keeping the blades on the upper rotor untwisted. With only a small increase in $\theta_{tw}^{l}$ (i.e., until just $\theta_{tw}^{l} = -3^\circ$), the inflow distribution was found to decrease on both rotors. For $\theta_{tw}^{l} > -3^\circ$, the inflow increased inboard on both rotors and was reduced slightly outboard on the lower rotor; see Figs. 17(a) and 17(b). The thrust distribution became more biased to the inboard regions of the blade when using larger blade twists. However, the

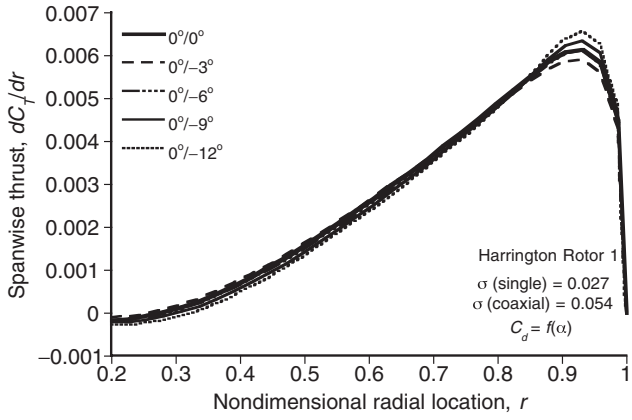


**(a) Upper rotor**

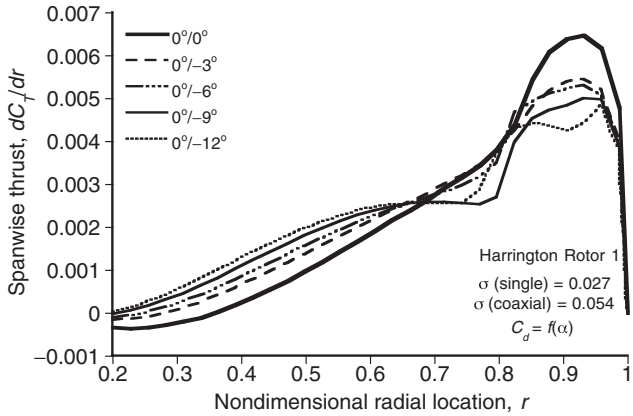


**(b) Lower rotor**

**Fig. 18. Variation of the spanwise thrust distribution on the upper and lower rotors as a function of the blade twist rate on the lower rotor (Harrington Rotor 1).**

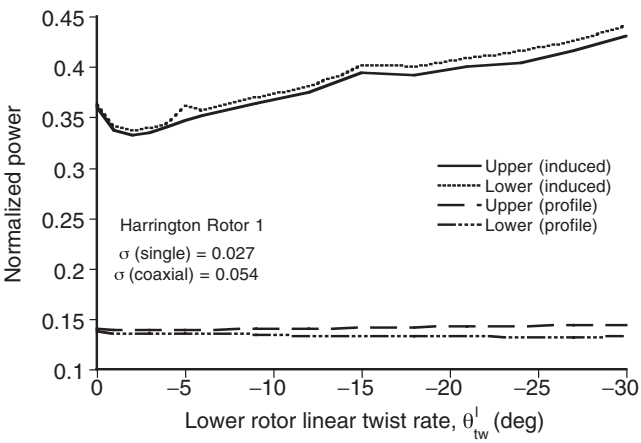


**Fig. 19. Variation of the induced and profile power contributions on the upper and lower rotors as a function of the blade twist rate on the lower rotor (Harrington Rotor 1).**

corresponding thrust and its grading did not change significantly on the upper rotor; see Figs. 18(a) and 18(b). In this case, the integrated induced power reached a minimum for a blade twist of $-3^\circ$ and then it increased rapidly; see Fig. 19. The corresponding profile power on both the rotors

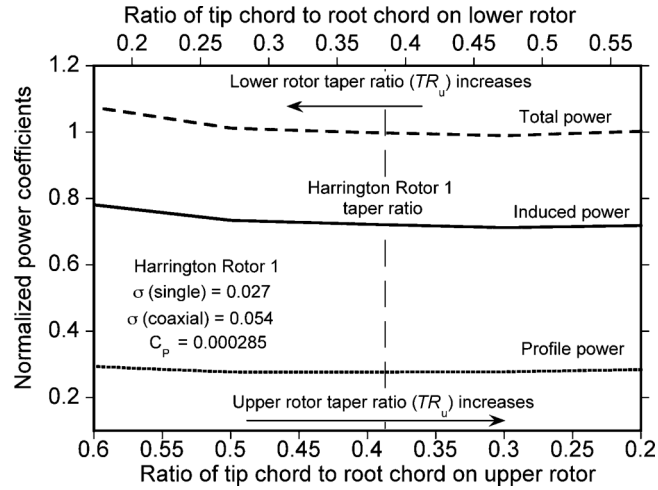


**Fig. 20. Variation of the normalized system induced, profile, and net power with changes in blade taper (Harrington Rotor 1).**

remained almost constant, as shown in Fig. 19. The total system power coefficient also reached a minimum when using a value of $\theta_{tw}^{l} = -3^\circ$ on the lower rotor.

*Blade planform.* Variations in blade planform were obtained by changing the relative solidity of the upper and lower rotors and the linear taper ratio of each set of blades, keeping all other design parameters constant. The solidity can be expressed as a function of the taper ratio, $TR$, of the blade, the point $r_t$ being where the taper starts and the root chord being $c_0$. Defining the $TR$ as the ratio of $c_0/c_1$, where $c_1$ is the blade tip chord, the thrust-weighted solidity of the coaxial as a system is obtained from the sum $\sigma_e^{\text{coax}} = \sigma_e^{\text{u}} + \sigma_e^{\text{l}}$, where the equivalent thrust-weighted solidity for either blade is

$$\sigma_e = \frac{3N_b}{\pi R}\int_0^1 c(r)\, r^2 dr \tag{8}$$

The resulting chord distribution on the blades is given by

$$c(r) = \begin{cases} c_0 & \text{for } r \le r_t \\ c_0\left[1 + \left(\dfrac{TR^{-1}-1}{1-r_t}\right)(r - r_t)\right] & \text{for } r > r_t \end{cases} \tag{9}$$

For the Harrington Rotor 1 system (the taper ratio is about 3:1), the solidity of each rotor is 0.027. With an increase in the taper on the upper rotor the profile power was found to decrease, whereas the profile power on the lower rotor increased as its taper ratio was decreased while maintaining a constant total thrust weighted solidity. It was also noted that the induced power on the upper rotor increased with an increase in the taper ratio and that the power (induced) decreased on the lower rotor. As a consequence, the total induced and profile power components of the coaxial as a system remained relatively insensitive to changes in $TR$; see Fig. 20. Notice again that the powers were normalized by the total power of the baseline rotor. Therefore, it is clear that the performance of the coaxial is determined primarily by the total solidity of the system and less so by unequal weighting of the solidities of the upper and lower rotors.

The corresponding variation of blade loading coefficients ($C_T/\sigma_e$) with a blade taper ratio is shown in Fig. 21. For the baseline rotor (which has equal solidities on the upper and lower rotors), it has been explained previously why the upper rotor carries a higher fraction of the total thrust. Therefore, its $C_T/\sigma_e$ is also higher than on the lower rotor. This means that the upper rotor will dictate the stall margins of the coaxial rotor

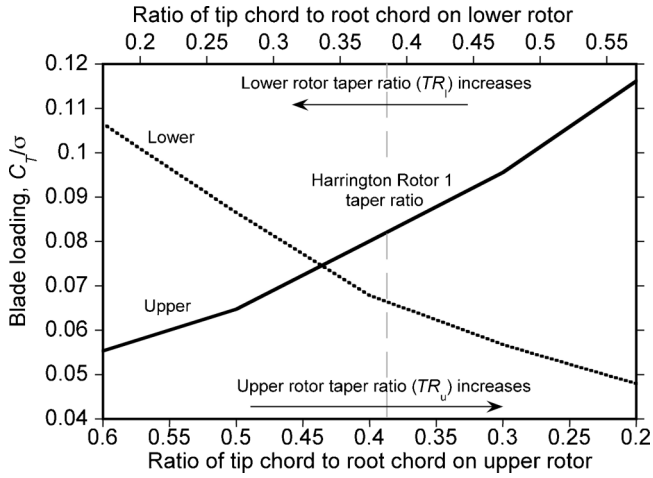


**Fig. 21. Variation of blade loading coefficient with changes in blade taper (Harrington Rotor 1).**

system and that the aerodynamic performance will be more limited than if both rotors were to reach their stall limits simultaneously. Therefore, to maximize overall stall margins for propulsion and maneuver capability, an optimum coaxial rotor should be designed such that the values of $C_T/\sigma_e$ are more equally balanced between the upper and lower rotors.

Figure 21 shows that the values of $C_T/\sigma_e$ on the upper and lower rotors can be made exactly equal (i.e., $C_T/\sigma_e = 0.075$ in this case) when blade taper ratios of 2.3:1 (i.e., $\sigma_e^u = 0.029$) and 2.8:1 (i.e., $\sigma_e^l = 0.025$) are used on the upper and lower rotors, respectively. (For the baseline rotor in this case, the value of $C_T/\sigma_e$ was 0.082 on the upper rotor.) Even with these changes in planform and solidity, the overall performance of the resulting rotor design was found to be essentially the same as for the baseline rotor.

## Optimization

The forgoing parametric studies were limited to simple blade shapes. Another goal of the present work was to study more complex blade shapes using a formal optimization method in an attempt to find the best rotor design with the minimum expenditure of computational costs and time, i.e., without having to commit to such extensive (and expensive) parametric studies.

*Blade shape functions.* Because of the different aerodynamic conditions on the upper and lower rotors, it is clear that the optimum blade twist should be different on both rotors if the best performance of the coaxial is to be obtained. Indeed, it has already shown theoretically (Refs. 16, 17) that the blade twist needed on the upper and lower rotors will not be the same if the best aerodynamic efficiency is the goal. In this respect, the baseline coaxial system can be referred to as a twin coaxial system because the blade geometry is the same for both rotors.

*Linear twist distributions.* The design variable vector in this case consisted of linear twist values on the upper and lower rotors, i.e.,

$$\mathbf{X} = \left\{\theta_{\text{tw}}^u,\ \theta_{\text{tw}}^l\right\}^T \tag{10}$$

The blade twist distributions on the upper and lower rotors are

$$\theta^u(r) = \theta_0^u + \theta_{\text{tw}}^u r \tag{11}$$

and

$$\theta^l(r) = \theta_0^l + \theta_{\text{tw}}^l r \tag{12}$$

where $\theta_0^u$ and $\theta_0^l$ are the collective pitch values on the upper and lower rotors, respectively.

*Piecewise linear twist distributions.* Because of the rotor-on-rotor interference effects, the use of linear blade twist may not minimize the induced losses. Therefore, the blades on the lower rotor were allowed to take other forms such as piecewise linear distributions, the design vector in this case being

$$\mathbf{X} = \left\{\theta_{\text{tw}_1}^u,\ \theta_{\text{tw}_2}^u,\ \theta_{\text{tw}_1}^l,\ \theta_{\text{tw}_2}^l,\ r_b^u,\ r_b^l\right\}^T \tag{13}$$

The resulting twist distributions on both blade sets are

$$\theta(r) = \begin{cases} \theta_0 + \theta_{\text{tw}}^1 r & \text{if } r \le r_b \\ \theta_0 + \theta_{\text{tw}}^1 r_b + \theta_{\text{tw}}^2 (r - r_b) & \text{if } r > r_b \end{cases} \tag{14}$$

*Blade planform.* The blade planform is described by Eq. (9). The design vector in this case can be written as

$$\mathbf{X} = \left\{TR^u,\ r_t^u,\ c_0^u,\ TR^l,\ r_t^l,\ c_0^l\right\}^T \tag{15}$$

where $TR^u$ and $TR^l$ are the taper ratios of the upper and lower rotors, respectively. The parametric studies of the effects of blade planform have suggested that the performance of a coaxial is relatively insensitive to changes in blade planform, other than how solidity weighting affects stall margins. Therefore, other than for solidity variations, these design variables (in Eq. (15)) were not included into the formal optimization problem. Note that if blade planform was included in the optimization process such as for solidity variations, a constraint should be added to maintain the net thrust-weighted solidity of the system.

*Interrotor spacing.* The induced losses obtained (in both hovering and forward flight conditions) will depend upon the interrotor spacing, $s/R$. In hovering flight, the wakes from the two rotors interact with each other and in this case the induced losses from rotor-on-rotor interference are generally the highest (Ref. 15). At higher forward speeds, the interaction between the wakes of the two rotors are reduced somewhat and the induced interference losses become progressively smaller. Therefore, higher values of $s/R$ are usually desired to limit induced losses in hovering flight. However, greater values of $s/R$ generally increases the parasitic drag of the rotor in forward flight because of the exposed shaft and blade pitch controls. It is recognized that in practice the final design value of $s/R$ may need to be chosen based on factors other than hover performance, as previously discussed.

*Constraints.* Various constraints are used to restrict the optimizer from picking blade designs that drive the solution into a nonphysical domain. In the present work, the following constraints were applied:

*Behavior constraints.* The behavior constraints are the inequality constraints that define the physical nature of the problem. In the present study, the requirement was to obtain a trimmed rotor solution by reducing the solution function evaluations. These conditions were modeled mathematically as two behavior constraints:

*1) Trim constraint:* For the design chosen, this constraint determines whether or not the rotors can be trimmed to the required thrust and/or to the torque-balanced operating state. To this end, the maximum number of iterations allowed for trim was limited to 20. With an initial collective pitch value being provided by the BEMT, the FVM usually converges in three to seven iterations. The constraint in this case is defined by

$$g_1(\mathbf{X}) = \text{I} - \text{I}_{\max} \le 0 \tag{16}$$

where $I_{\max}$ is the maximum number of iterations allowed for trim (set to 20 for the present study) and $I$ is the number of iterations actually taken to trim the rotors. If $g_1(\mathbf{X}) \le 0$, then the rotor is trimmed and the design is in the feasible region. When $g_1(\mathbf{X}) > 0$, the constraint is not

satisfied and the rotor design is infeasible, so the optimizer updates the blade shapes to bring the solution back into the feasible region.

*2) FM constraint:* The second aerodynamic constraint is that the figure of merit of the coaxial rotor should always be less than unity. Because an objective can be to maximize the *FM*, the optimizer can sometimes try to choose nonphysical blade designs. The *FM* constraint is, therefore, defined by

$$g_2(\mathbf{X}) = FM - 1 \leq 0 \tag{17}$$

*Side constraints.* Side constraints set the lower and upper bounds on the design variables and limit the overall design space. The upper and lower side constraints (i.e., $\mathbf{X}^u$ and $\mathbf{X}^l$, respectively) were set to limit the maximum blade twist to $+5^\circ$ and the minimum (nose-down) twist to $-40^\circ$. Other side constraints were imposed, where and when needed.

**Blade twist optimization**

As an example of the approach, the baseline rotor considered in the present optimization study was the Harrington Rotor 1 system, which has untwisted blades that are linearly tapered in planform.

*Linear blade twist.* For this case, the blade shape functions were defined by linear twist rates, as given by Eqs. (10–12). The objective was to maximize the system *FM* (i.e., Eq. (7)) with the imposition of the constraints (Eqs. (16) and (17)). To validate the numerical coupling between the aerodynamic solutions and the optimization algorithm, parametric computations were first performed using the BEMT with blade twist values ranging from between $+9^\circ$ and $-27^\circ$. The results showed that the blade design with $(\theta^u_{\text{tw}}, \theta^l_{\text{tw}}) = (-9^\circ, -12^\circ)$ gave the maximum value of *FM*, but this value was only 3% higher than that calculated for the baseline rotor (i.e., $FM = 0.563$). However, the optimum from the BEMT (which is a linear solution) may not be same as that when using the FVM, which is considered next.

Further parametric results were obtained using the FVM by varying the linear twist on both rotors from $0^\circ$ to $-30^\circ$ in steps of $-3^\circ$; Fig. 22 shows a contour map of the resulting variations in the *FM*. As previously explained, because of the inherent aperiodicity in the flow through a coaxial rotor, the objective function was computed by ensemble averaging the *FM* over five rotor revolutions after trim was obtained.

Notice from Fig. 22 that a higher *FM* can be obtained by increasing the blade twist on the upper rotor to about $-18^\circ$ or $-20^\circ$. For higher nose-down blade twist rates, there is a range of $\theta^l_{\text{tw}}$, i.e., from $0^\circ$ to $-15^\circ$, for which the *FM* is higher, which shows that for larger values of $\theta^u_{\text{tw}}$ the *FM* (or total power) is relatively insensitive to the blade twist used on the lower rotor. Therefore, there exist multiple local optima (as shown) but only one global optima, i.e., $(\theta^u_{\text{tw}}, \theta^l_{\text{tw}}) = (-18^\circ, -3^\circ)$ with a resulting *FM* of 0.6585 in this case (i.e., a 17% increase over the baseline rotor).

The foregoing parametric study showed that the value of *FM* for a coaxial is a nonconvex function of blade twist. The use of the total power coefficient $C_P$ as the objective function was also considered, which provided similar results. Notice that the multiple pockets of higher *FM* in Fig. 22 bring out the inherent nonconvexity of the problem. This means that any optimization process will critically depend upon the initial blade design selected for the optimization. To this end, several initial designs were analyzed and the optima obtained were compared to each other to establish the global optimum.

Results are now presented to show how the process of optimization depends upon the initial design chosen. For the first case, the initial blade twist was $\mathbf{X}^0 = \{-20^\circ, -20^\circ\}^T$ and the resulting optimum twist was $\mathbf{X}^* = \{-19^\circ, -8.5^\circ\}^T$ giving a rotor *FM* of 0.655, which is a 16% gain over the baseline. For the second case, the initial design was $\mathbf{X}^0 = \{-15^\circ, -5^\circ\}^T$ and the resulting optimum blade twist rates were $\mathbf{X}^* = \{-17.26^\circ, -3.08^\circ\}^T$ with an *FM* of 0.6588, which was a gain of 17% over the baseline coaxial. Compared to the BEMT, it was found that the optimum blade shape given by the FVM leads to a requirement for more blade twist on the upper rotor compared to that used on the lower rotor.

The paths followed by the optimizer to find optimum blade shape for these two cases is shown in Fig. 23. These results are consistent with the parametric study, which also suggested the optimum values of blade twist were about $-18^\circ$ on the upper rotor and $-3^\circ$ on the lower rotor. However, the nonconvexity of this problem with just two design variables (i.e., linear twist rates on the upper and lower rotors) suggests that the more general optimization problem may prove to be very challenging.

*Piecewise linear twist.* The shape function for each blade in this case composed of a breakpoint and different twist rates defined before and after these breakpoints. The corresponding design vector is

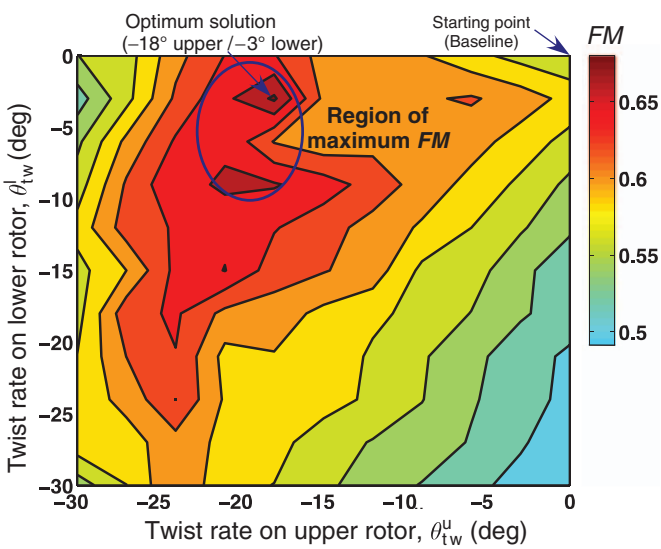


**Fig. 22. Contour plot of *FM* as a function of linear blade twist on the upper and lower rotors (results produced by the FVM).**

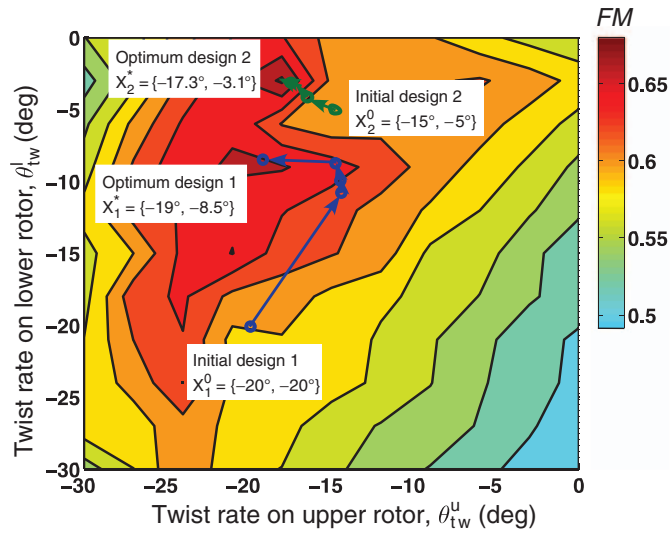


**Fig. 23. Representation of the paths followed by the optimizer in the *FM* domain when using different initial blade designs.**

given by Eq. (13) and the twist distribution is given by Eq. (14). As with the two-design variable problem, several initial designs were considered to test for the local optima. Three cases were found to have the highest values of *FM*. *Result 1*: The initial design was $\mathbf{X}^0 = \{-15^\circ, -15^\circ, -15^\circ, -15^\circ, 0.5, 0.5\}^T$, and the optimum design was $\mathbf{X}^* = \{-17.2^\circ, -17.8^\circ, -8.6^\circ, -6.2^\circ, 0.496, 0.432\}^T$ with a *FM* of 0.668, which was a 19% gain over the baseline coaxial. The optimum blade design in this case had almost linear twist distributions on both the rotors. However, the blades of the lower rotor had less twist compared to the upper rotor, as found previously. *Result 2*: The initial rotor design was $\mathbf{X}^0 = \{-21^\circ, -18^\circ, -3^\circ, -3^\circ, 0.8, 0.8\}^T$, and the optimum design was $\mathbf{X}^* = \{-19.7^\circ, -18.3^\circ, -2.9^\circ, -2.8^\circ, 0.94, 1.0\}^T$ with a *FM* of 0.6651, which was an 18% gain. This result corresponded to almost linear twist distributions over both sets of blades. *Result 3*: The initial rotor design in this case was $\mathbf{X}^0 = \{-20^\circ, -15^\circ, -20^\circ, -15^\circ, 0.5, 0.5\}^T$, and the optimum was $\mathbf{X}^* = \{-24.4^\circ, -18.3^\circ, -19.5^\circ, -8.8^\circ, 0.82, 0.86\}^T$ with an *FM* that was 20% higher compared to the baseline. However, in this case the blade loads (as well as thrust and power) showed higher fluctuations from wake interactions and so this design may not be a practical choice.

The foregoing results show that for most of the optimization studies conducted with bilinear blade twist rates (and starting from different initial designs), the optimum blade twist was higher on the upper rotor compared to the lower rotor. This result was also obtained from the parametric studies (see Fig. 22), which suggested that for higher blade twist rates the performance was relatively insensitive to the blade twist used on the lower rotor. Therefore, the approach resulted in multiple optima. Finally, as was found previously from the BEMT analysis, the FVM confirms that there is no one blade twist design that necessarily gives the best hovering performance for a coaxial rotor (at least not for the one considered in this case) and that several blade shapes may give comparable levels of efficiency.

## Conclusions

Methods of making profitable blade designs to maximize the performance of coaxial rotors in hovering flight have been explored. The results show significant latitude in the design of a coaxial rotor for good aerodynamic efficiency, but the maximum achievable efficiency will critically depend on the imposed geometric and other constraints. The achievable system efficiency of a coaxial is limited primarily by the induced losses incurred on the lower rotor by the influence of the wake of the upper rotor. However, the efficiency of a coaxial can still be improved significantly by striving to find an optimum set of blade shapes that will minimize interference losses on both rotors, even though the two rotors may turn out to be geometrically different. In the present study, emphasis was placed on the optimization of the blade twist, planform shape, and interrotor spacing, although other design variables can be included within the optimization framework. The key conclusions from the present work are as follows:

1) The performance of the coaxial rotor considered was shown to be nonlinear functions of the twist rates used on the blades of both the upper and lower rotors. For the coaxial configuration studied, efficiency was notably increased by increasing the blade twist on the upper rotor but more insensitive to blade twist on the lower rotor. It was also shown that using linear blade twist provided almost the same improvements in performance compared bilinear variations of twist. While quantitatively different results may be obtained with other rotors and/or with other interrotor spacings, the present results suggest that to extract maximum efficiency of a coaxial rotor different blade twist distributions will be required on the upper and lower rotors.

2) For the coaxial rotor considered, its aerodynamic efficiency was found to be relatively insensitive to changes in blade planform, i.e., taper. However, it was also shown that the upper and lower rotors may still have to be designed with different planforms (e.g., with different solidities) to maximize or improve the net stall margins of the coaxial as a system. To this end, at a torque-balanced condition (i.e., the normal operating state for a coaxial) the upper rotor of the pair must generally be designed with a higher value of solidity.

3) Increasing the interrotor spacing has been shown to reduce aerodynamic interference losses between the upper and lower rotors of a coaxial. Specifically, the inflow was increased on the inboard regions of the lower rotor and decreased on outboard regions. Practically, rotor spacing must also be chosen based on allowances for differential blade flapping (i.e., depending on the hub design, blade stiffness), and the parasitic drag minimization of the rotor shaft when in edgewise forward flight. Such constraints will always limit the range of allowable solutions for the blade shapes that might otherwise be suggested by an isolated rotor analysis.

4) For smaller interrotor spacings (such as those used on the Harrington coaxial system), the lower rotor was shown to significantly affect the performance of the upper rotor through aerodynamic interactions. These types of interference effects cannot be predicted from within the linearized framework of the momentum theory. While the free-vortex wake method offers many advantages in the analysis of a coaxial rotor (e.g., good fidelity at moderate computational cost), ultimately CFD may provide further insight into the interdependent aerodynamic effects that arise from nonlinear rotor-on-rotor interference effects.

5) The blade shape optimization of a coaxial rotor for the best levels of aerodynamic efficiency was found to be a nonconvex problem. Therefore, the optimization process may have to be repeated several times to cover the entire design space and uncover the rotor design that gives the best efficiency, the optimum being dependent to some extent on the initial blade design that is chosen. In fact, the nonconvexity of the problem may limit the usefulness of formal optimization methods to significantly accelerate the design process, and extensive (and expensive) parametric studies may still be required.

## Acknowledgments

This work was supported by a contract from the Office of Naval Research. The technical Monitors were John Kinzer and Judah Milgram. The authors are grateful for the discussions with their many professional colleagues, including the technical contributions of Shreyas Ananthan to this work.

## References

[1]Bagai, A., "Aerodynamic Design of the X2 Technology Demonstrator Main Rotor Blade," American Helicopter Society International 64th Annual Forum Proceedings, Montréal, Canada, April 28–May 1, 2008.

[2]Preator, R., Leishman, J. G., and Baldwin, G. D., "Performance and Trade Studies of Mono Tiltrotor Design," American Helicopter Society International 61st Annual Forum Proceedings, Grapevine, TX, June 1–3, 2005.

[3]Pines, D. J., and Bohorquez, F., "Challenges Facing Future Micro-Air-Vehicle Development," *Journal of Aircraft*, Vol. 43, (2), March–April 2006, pp. 290–305.

[4]Chaney, M. C., "The ABC Helicopter," *Journal of the American Helicopter Society*, 14, (4), October 1969, pp. 10–19.

[5]Paglino, V. M., "Forward Flight Performance of a Coaxial Rigid Rotor," American Helicopter Society 27th Annual Forum Proceedings, Washington DC, May 19–21, 1971.

[6]Playle, S. C., Korkan, K. D., and von Lavante, E., "A Numerical Method for the Design and Analysis of Counter-Rotating Propellers," *Journal of Propulsion and Power*, Vol. 2, (1), January–February 1986, pp. 57–63.

[7]Leishman, J. G., "Aerodynamic Performance Considerations in the Design of a Coaxial Proprotor," *Journal of the American Helicopter Society*, **54**, 012005 (2009).

[8]Coleman, C. P., "A Survey of Theoretical and Experimental Coaxial Rotor Aerodynamic Research," 19th European Rotorcraft Forum Proceedings, Cernobbio-Como, Italy, September 14–16, 1993. Also published as NASA TP-3675, March 1997.

[9]McAlister, K. W., Tung. C., Wilson, J. S., and Rand, O., "Experimental and Numerical Study of a Model Coaxial Rotor," American Helicopter Society International 62nd Annual Forum Proceedings, Phoenix, AZ, May 9–11, 2006.

[10]McAlister, K. W., and Tung. C., "Experimental Study of a Hovering Coaxial Rotor with Highly Twisted Blades," American Helicopter Society International 64th Annual Forum Proceedings, Montréal, Canada, April 29–May 1, 2008.

[11]Andrew, M. J., "Coaxial Rotor Aerodynamics in Hover," *Vertica*, Vol. 5, 1981, pp. 163–172.

[12]Saito, S., and Azuma, S., "A Numerical Approach to Coaxial Rotor Aerodynamics," 7th European Rotorcraft Forum Proceedings, Garmisch–Partenkirchen, Germany, September 8–11, 1981.

[13]Zimmer, H., "The Aerodynamic Calculation of Counter Rotating Coaxial Rotors," 11th European Rotorcraft Forum Proceedings, London, UK, September 10–13, 1985.

[14]Valkov, T., "Aerodynamic Loads Computation on Coaxial Hingeless Helicopter Rotors," Paper AIAA 90-0070, 28th Aerospace Sciences Meeting, Reno, NV, January 8–11, 1990.

[15]Leishman, J. G., and Syal, M., "Figure of Merit Definition for Coaxial Rotors," *Journal of the American Helicopter Society*, Vol. 53, (3), July 2008, pp. 290–300.

[16]Leishman, J. G., and Ananthan, S., "An Optimum Coaxial Rotor System for Axial Flight," *Journal of the American Helicopter Society*, Vol. 53, (4), October 2008, pp. 366–381.

[17]Rand, O., and Khromov, V., "Aerodynamic Optimization of Coaxial Rotor in Hover and Axial Flight," 27th International Congress of the Aeronautical Sciences, Nice, France, September 19–24, 2010.

[18]Bourtsev, B. N., Vainstein, I. M., and Petrosian, E. A., "Phenomenon of a Coaxial Helicopter High Figure of Merit at Hover," 23rd European Rotorcraft Forum Proceedings, Dresden, Germany, September 16–18, 1997.

[19]Kim, H. W., and Brown, R. E., "Coaxial Rotor Performance and Wake Dynamics in Steady and Maneuvering Flight," American Helicopter Society International 62nd Annual Forum Proceedings, Phoenix, AZ, May 9–11, 2006.

[20]Lakshminarayan, V. K., and Baeder, J. D., "High-Resolution Computational Investigation of Trimmed Coaxial Rotor Aerodynamics in Hover," *Journal of the American Helicopter Society*, **54**, 042008 (2009).

[21]Gessow, A., "Effect of Rotor-Blade Twist and Plan-Form Taper on Helicopter Hovering Performance," NACA Technical Note 1542, 1948.

[22]Gessow, A., and Myers, G. C., *Aerodynamics of the Helicopter*, MacMillan Co., New York, NY, 1952, pp. 73–75.

[23]Leishman, J. G., *Principles of Helicopter Aerodynamics*, 2nd ed., Cambridge University Press, New York, NY, 2006.

[24]Lock, C. N. H., Bateman, H., and Townend, H. C. H., "Experiments to Verify the Independence of the Elements of an Airscrew Blade," British ARC R & M 953, 1924.

[25]Lock, C. N. H., "Interference Velocity for a Close Pair of Contra-Rotating Airscrews," British R & M No. 2084, July 1941.

[26]Leishman, J. G., Bhagwat, M. J., and Bagai, A., "Free-Vortex Filament Methods for the Analysis of Helicopter Rotor Wakes," *Journal of Aircraft*, Vol. 39, (5), September–October 2002, pp. 759–775.

[27]Bhagwat, M. J., and Leishman, J. G., "Stability, Consistency and Convergence of Time-Marching Free-Vortex Rotor Wake Algorithms," *Journal of the American Helicopter Society*, Vol. 46, (1), January 2001, pp. 59–71.

[28]Bhagwat, M., and Leishman, J. G., "Accuracy of Straight-Line Segmentation Applied to Curvilinear Vortex Filaments," *Journal of the American Helicopter Society*, Vol. 46, (2), April 2001, pp. 166–169.

[29]Bhagwat, M. J., and Leishman, J. G., "Generalized Viscous Vortex Core Models for Application to Free-Vortex Wake and Aeroacoustic Calculations," American Helicopter Society International 58th Annual Forum Proceedings, Montréal Canada, June 11–13, 2002.

[30]Ananthan, S., and Leishman, J. G., "Role of Filament Strain in the Free-Vortex Modeling of Rotor Wakes," *Journal of the American Helicopter Society*, Vol. 49, (2), April 2004, pp. 176–191.

[31]Beddoes, T. S., "Representation of Airfoil Behavior," *Vertica*, Vol. 7, (2), 1983, pp. 183–197.

[32]Ananthan, S., "Analysis of Rotor Wake Aerodynamics During Maneuvering Flight Using a Free-Vortex Wake Methodology," Ph.D. Thesis, University of Maryland, College Park, MD, 2006.

[33]Syal, M., and Leishman, J. G., "Aerodynamic Optimization Study of a Coaxial Helicopter Rotor," American Helicopter Society 65th Annual Forum Proceedings, Grapevine, TX, May 27–29, 2009.

[34]Nocedal, J., and Wright, S. J., *Numerical Optimization*, Springer, NY, 2006.

[35]Vanderplaats, G. N., *Numerical Optimization Techniques for Engineering Design*, McGraw-Hill, Inc., New York, NY, 1984.

[36]Harrington, R. D., "Full-Scale Tunnel Investigation of the Static Thrust Performance of a Coaxial Helicopter Rotor," NACA Technical Note 2318, 1951.

[37]Taylor, M. K., "A Balsa-Dust Technique for Air-Flow Visualization and Its Application to Flow through Model Helicopter Rotors in Static Thrust," NACA Technical Note 2220, 1950.

[38]Buning, P., "Consolidation of Time-Accurate, Moving Body Capabilities in OVERFLOW," 6th Overset Composite Grid and Solution Technology Symposium, Ft. Walton Beach, FL, October 8–10, 2002.

[39]Juhasz, O., Syal, M., Celi, R., Khromov, V., Rand, O., Ruzicka, G. C., and Strawn, R. C., "A Comparison of Three Coaxial Aerodynamic Prediction Methods Including Validation with Model Test Data," 2010 AHS Aeromechanics Specialists Conference, San Francisco, CA, January 20–22, 2010.